Molecular dynamics simulation of hydrocarbon molecules in condensed phases. II. Benzene

Jon Anderson, John J. Ullo, and Sidney Yip

Citation: J. Chem. Phys. **86**, 4078 (1987); doi: 10.1063/1.452748
View online: http://dx.doi.org/10.1063/1.452748
View Table of Contents: http://jcp.aip.org/resource/1/JCPSA6/v86/i7
Published by the American Institute of Physics.

Molecular dynamics simulation of hydrocarbon molecules in condensed phases. II. Benzene

Jon Anderson[a)]
Department of Nuclear Engineering, Massachusetts Institute of Technology, Cambridge, Massachusetts 02139

John J. Ullo
Schlumberger–Doll Research Ridgefield, Connecticut 06877-4108

Sidney Yip
Department of Nuclear Engineering, Massachusetts Institute of Technology, Cambridge, Massachusetts 02139

(Received 15 October 1986; accepted 18 December 1986)

Molecular dynamics simulations of liquid (305 K) and solid (10 K) benzene have been carried out to investigate the vibrational properties of benzene in the condensed phase. The benzene molecule is modeled as a fully flexible system of 12 atoms with intramolecular interactions based on *ab initio* harmonic potentials and intermolecular interactions given by semiempirical atom–atom potentials. Vibrational frequencies are analyzed in terms of the frequency spectrum of the velocity autocorrelation function and the results are found to correlate well with optical absorption and scattering data. Single particle density fluctuations are calculated over a range of wave numbers and results are obtained that can be directly compared to the intensity distributions of inelastically scattered thermal neutrons. The different comparisons indicate that the existing potential energy function provides an essentially quantitative description of molecular vibrations of benzene.

I. INTRODUCTION

Of the many physical properties of a molecular system which are useful for the study of interatomic forces, vibrational frequencies and amplitudes are among the most important. Given a force field model for a particular system, one can test its validity by calculating the vibrational properties with as few assumptions as possible and comparing the results with such experimental data as infrared and Raman frequencies and the amplitude-sensitive spectra observed by inelastic scattering of thermal neutrons. In practice, one's ability to attribute a discrepancy in the comparison to an inadequacy in the force field depends on the accuracy with which the relevant dynamics of the system can be determined once the force field is prescribed.

A general method of determining the physical properties of a molecular model with well-defined forces is molecular dynamics (MD) simulation. This technique is well established for the study of statistical mechanical properties of atomic systems and systems with rigid molecular units[1]; its extension to polyatomics with explicit intra- and intermolecular interactions has also been discussed recently.[2,14] A fundamental feature of the MD approach is that it gives the dynamical solutions to the classical many-body problem with no assumptions (in principle) once the forces are specified. In contrast to conventional normal mode analysis, MD is valid at any temperature and is equally applicable to solids and liquids.

In this paper, we report an MD study of the vibrational properties of benzene (C_6H_6). There exist several simulations of this system, all treating the molecule as a rigid, planar hexagon.[3–8] Evans and Watts[3] investigated structural properties by means of Monte Carlo simulation using a six center Lennard-Jones (6-12) potential.[9] This potential was later used by Steinhauser[4] in an MD study of liquid structure,[10] and improved versions were employed by Claessens *et al.*[5] and Adan *et al.*[6] Most recently Linse and coworkers[7,8] have carried out Monte Carlo and MD simulations of solid and liquid benzene using an *ab initio* atom–atom intermolecular pair potential developed by Karlstrom *et al.*[11] In these simulations, interest was centered on thermodynamic, structural, and translational and rotational diffusion properties.

Our work differs from previous simulations of benzene in three key aspects. First, all 36 atomic degrees of freedom of the molecule are treated as dynamical variables; i.e., we go beyond the rigid molecule approximation and treat the benzene molecule as fully flexible. Secondly, a realistic potential model is used, this being a combination of harmonic potentials in the internal coordinates determined from *ab initio* Hartree–Fock calculations[12] and atom–atom potentials for the intermolecular interactions determined by fitting neutron data[13] on phonon dispersion curves. Lastly our investigation extends to the calculation of the single particle dynamic structure factor, thus demonstrating the feasibility of utilizing directly neutron inelastic scattering spectra. From our study the emergent conclusion is that the existing potential function for benzene is sufficiently accurate for general applications of MD simulations. In a comparison study of *n*-butane (C_4H_{10}) using a transferable force field optimized for an entire family of linear alkanes, we have found results that

[a)] Present address: AT&T Bell Laboratories, Holmdel, N.J. 07733.

 0021-9606/87/074078-12$02.10

are less satisfactory and thus indicate a certain deficiency in that potential model.[14]

Our potential model which considers intra- and intermolecular interactions is specified in the next section. In Sec. III, some MD computational details are briefly discussed. Here we present a method that simplifies the force calculations for the intramolecular potential functions which are expressed in molecular internal coordinates.[15] Equilibration aspects are also discussed. Results of property calculations are presented in Sec. IV. These include the generalized vibrational frequency spectra and the van Hove self-correlation functions for the liquid and solid phases. Some structural and mean-square displacement results are also discussed. Concluding remarks are given in Sec. V.

II. BENZENE MODEL

In the present study the benzene molecular potential energy function is specified as a combination of *ab initio* intramolecular interactions and semiempirical atom–atom intermolecular interactions. The former is obtained from a ground-state harmonic potential function developed for benzene by Pulay *et al.*[12] In general, the intramolecular potential function for a polyatomic molecule can be expressed as

$$\phi_{\text{intra}}(\mathbf{R}) = \phi_S(\mathbf{R}) + \phi_B(\mathbf{R}) + \phi_w(\mathbf{R}) + \phi_T(\mathbf{R}) + \phi_C(\mathbf{R}), \quad (1)$$

where ϕ_S is the atom–atom bond stretching contribution, ϕ_B and ϕ_w are the in-plane and out-of-plane (wag) bond angle bending contributions, respectively, ϕ_T is the torsional potential associated with dihedral angle bending, and ϕ_C represents cross terms for the $\phi_S\phi_B$ in-plane interactions and $\phi_w\phi_T$ out-of-plane interactions. The vector $\mathbf{R}$ has as its components all the internal coordinates for the entire molecule (see below).

The equilibrium molecular structure of benzene (Fig. 1) is known to be planar with the six carbon (C) and six hydrogen (H) atoms at the corners of a concentric, regular hexagon.[16] The equilibrium bond lengths specified in the intramolecular force field are: $r_{CC} = 1.395$ Å, $r_{CH} = 1.077$ Å.[12] These lengths are slightly smaller compared to the accepted experimental values, $r_{CC} = 1.397$ Å, $r_{CH} = 1.084$ Å.[16] In the present benzene model the force field values are the ones used.

The internal coordinates used in the benzene intramolecular potential model are summarized in Table I and are

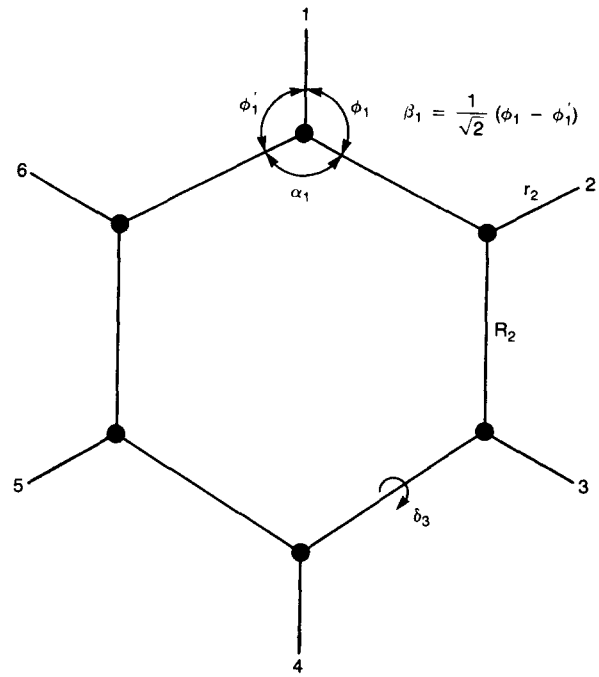

FIG. 1. Benzene geometry.

defined as follows: r_1 corresponds to the C_1H_1 bond length, R_1 is the C_1C_2 bond length, ϕ_1' and ϕ_1 refer to the $C_6C_1H_1$ and $H_1C_1C_2$ in-plane bond angles, respectively, α refers to the $C_6C_1C_2$ in-plane bond angle, γ_1 is the C_1H_1 out-of-plane (wag) bond angle, with the angle being positive if the H_1 atom is displaced in the positive z direction, and δ_1 corresponds to the $C_6C_1C_2C_3$ dihedral angle. The sign of the torsional coordinate δ_1 is defined as in Ref. 15. These definitions continue cyclically for all the internal coordinates. The symmetry coordinates β_i, q_{19}, q_{20a}, q_{20b}, q_{28}, q_{29a}, and q_{29b} are linear combinations of in-plane and torsional bond angles and are used to reduce redundant internal coordinates.

In terms of the internal coordinates, the intramolecular potential components in Eq. (1) for benzene are

$$2\phi_S(\mathbf{R}) = \sum_{i=1}^{6} k_r(r_i - r_0)^2 + \sum_{i=1}^{6} k_R(R_i - R_0)^2,$$

$$2\phi_B(\mathbf{R}) = \sum_{i=1}^{6} k_\beta(\beta_i)^2 + k_{q19}(q_{19})^2 + k_{q20a}(q_{20a})^2 + k_{q20b}(q_{20b})^2, \quad (2)$$

TABLE I. Internal coordinates for benzene.

No.	Coordinate	Description
1–6	$r_1,\ldots,r_6$	CH stretching
7–12	$R_1,\ldots,R_6$	CC stretching
13–18	$\beta_1 = 2^{-1/2}(\phi_1 - \phi_1'),\ldots,\beta_6$	CH in-plane deformation
19	$q_{19} = 6^{-1/2}(\alpha_1 - \alpha_2 + \alpha_3 - \alpha_4 + \alpha_5 - \alpha_6)$	B_{1u} deformation
20	$q_{20a} = 12^{-1/2}(2\alpha_1 - \alpha_2 - \alpha_3 + 2\alpha_4 - \alpha_5 - \alpha_6)$	E_{2g} deformation
21	$q_{20b} = 1/2(\alpha_2 - \alpha_3 + \alpha_5 - \alpha_6)$	
22–27	$\gamma_1,\ldots,\gamma_6$	CH wagging
28	$q_{28} = 6^{-1/2}(\delta_1 - \delta_2 + \delta_3 - \delta_4 + \delta_5 - \delta_6)$	B_{2g} deformation
29	$q_{29a} = 1/2(-\delta_1 + \delta_3 - \delta_4 + \delta_6)$	E_{2u} deformation
30	$q_{29b} = 12^{-1/2}(-\delta_1 + 2\delta_2 - \delta_3 - \delta_4 + 2\delta_5 - \delta_6)$	

TABLE II. Scaled *ab initio* harmonic force constants for benzene in the internal coordinate representation.

Potential energy term	Force constant k^a	Potential energy term	Force constant k^a
r_1^2	5.176	β_1^2	0.512
$r_1r_2(o)$	0.016	$\beta_1\beta_2(o)$	0.009
$r_1r_3(m)$	0.005	$\beta_1\beta_3(m)$	−0.010
$r_1r_4(p)$	0.001	$\beta_1\beta_4(p)$	−0.001
r_1R_1	0.079	β_2q_{20a}	−0.067
r_1R_2	−0.002	β_1q_{20b}	0.0774
r_1R_3	0.022	β_2q_{20b}	−0.0387
$r_1\beta_2(o)$	0.005	q_{19}^2	1.236
$r_1\beta_3(m)$	−0.007	q_{20a}^2	1.236
r_1q_{19}	−0.105	γ_1^2	0.4389
r_1q_{20a}	−0.099	$\gamma_1\gamma_2(o)$	−0.0690
r_2q_{20a}	0.0495	$\gamma_1\gamma_3(m)$	−0.0003
r_2q_{20b}	−0.0857	$\gamma_1\gamma_4(p)$	−0.0176
R_1^2	6.636	γ_1q_{28}	−0.1456
$R_1R_2(o)$	0.633	γ_1q_{29a}	0.1472
$R_1R_3(m)$	−0.442	γ_2q_{29a}	−0.0736
$R_1R_4(p)$	0.440	γ_2q_{29b}	−0.1275
$R_1\beta_1$	0.167	q_{28}^2	0.3763
$R_1\beta_3$	−0.010	q_{29a}^2	0.3156
$R_1\beta_4$	0.019	q_{29b}^2	0.3156
R_1q_{20a}	0.134		
R_2q_{20a}	−0.268		
R_1q_{20b}	0.2321		

[a] Units: energy in 10^{-18} J, coordinates in Å and rad.

$$2\phi_w(\mathbf{R}) = \sum_{i=1}^{6} k_\delta(\delta_i)^2,$$

$$2\phi_T(\mathbf{R}) = k_{q28}(q_{28})^2 + k_{q29a}(q_{29a})^2 + k_{q29b}(q_{29b})^2,$$

$\phi_C(\mathbf{R})$ = in-plane + out-of-plane cross terms.

Equation (1) can be summarized in a matrix notation,

$$2\phi_{\text{intra}}(\mathbf{R}) = (\mathbf{R} - \mathbf{R}_0)^T\mathbf{F}_R(\mathbf{R} - \mathbf{R}_0), \quad (3)$$

where $\mathbf{R}$ is the internal coordinate vector with elements defined in Table I, and subscript 0 denotes the equilibrium values of the internal coordinates, and $\mathbf{F}_R$ is the internal coordinate force constant matrix determined from *ab initio* Hartree–Fock calculations (see Table II).[12] A few empirical scale factors have been applied to the *ab initio* force constants to correct for systematic errors and to allow for the reproduction of a large number of observed vibrational frequencies.

The intermolecular interactions are based on semiempirical atom–atom pair potentials,

$$\phi_{\text{intra}}(r_{ij}) = A\exp(-\alpha r_{ij}) - Cr_{ij}^{-6}, \quad (4)$$

where r_{ij} is the distance between atoms i and j in different molecules, and the parameters A, α, and C depend on the type of i–j interaction, C–C, C–H, or H–H. The parameter values adopted are the refined Williams parameters[13] listed in Table III. The original Williams parameters[17,18] were obtained by weighted least squares fitting to experimental data (crystal structures, elastic constant, and sublimation energies) for several aromatic hydrocarbons. Powell and coworkers[13] have further refined the most accurate parameter set (Set IV in Ref. 18) using lattice vibrational frequency data obtained from coherent inelastic neutron scattering measurements on deuterated benzene. The resulting parameters have been shown to give an accurate reproduction of the observed lattice vibrational frequencies.[13]

TABLE III. Intermolecular potential parameters for benzene.

Interaction	Parameters[a] A	α	C
C–C	290.46	3.60	0.069
C–H	107.53	3.67	2.293
H–H	8.78	3.74	−0.184

[a] Units for A, α, and C are 10^{-18} J, Å^{-1}, and 10^{-18} J Å^6, respectively.

III. MD COMPUTATIONAL DETAILS

The MD simulation technique employed in this work utilizes the standard method[19] with modifications for treating the benzene molecular system as a system of carbon and hydrogen atoms. These modifications pertain specifically to the force evaluation and equilibrium of polyatomic molecules.

In the force evaluation the intermolecular forces are calculated in the usual manner using atom–atom pairwise-additive central potentials. However, because the intramolecular potential is described in terms of internal coordinates, calculation of the intramolecular forces from Cartesian gradients of the potential is not straightforward. Using techniques well known in molecular vibrational analysis,[15] we have devised a simplified method for calculating the intramolecular forces using potentials which are expressed in internal coordinates. Let $\mathbf{B}$ denote a transformation matrix between internal and Cartesian coordinate systems,

$$\mathbf{R} = \mathbf{BX}, \tag{5}$$

where $\mathbf{X} = (x_1, y_1, z_1, x_2, y_2, z_2, \ldots, x_{12}, y_{12}, z_{12})$ is a vector representing the Cartesian coordinates of the atoms in the benzene molecule. The elements of **B** are obtained by evaluating the analytic expressions derived for the benzene internal coordinates (see the Appendix). Using Eqs. (3) and (5) the intramolecular forces can be expressed as

$$\mathbf{f} = -\frac{d\phi_{\text{intra}}}{d\mathbf{R}}\frac{d\mathbf{R}}{d\mathbf{X}} = -(\mathbf{R}-\mathbf{R}_0)^T\mathbf{F}_R\mathbf{B}, \tag{6}$$

where use is made of the properties that the internal coordinate force constant matrix $\mathbf{F}_R$ is symmetric and that **B** is constant for a given **X**. The vector $\mathbf{R}_0$ is the equilibrium internal coordinate vector.

The elements of f are the Cartesian components of the intramolecular force, $\mathbf{f} = (f_{x_1}, f_{y_1}, f_{z_1}, f_{x_2}, f_{y_2}, f_{z_2} \cdots, f_{x_{12}}, f_{y_{12}}, f_{z_{12}})$. Including the intermolecular force contributions, the total force on the ith atom imposed by all the other atoms in the system is

$$\mathbf{F}_i = -\sum_j{}' \nabla_i \phi_{\text{inter}}(r_{ij}) + \mathbf{f}(i), \tag{7}$$

where the prime on the summation symbol denotes that $j = i$ is excluded from the sum, and $\mathbf{f}(i)$ represents the f_x, f_y, and f_z intramolecular force components for atom i.

During equilibration of the flexible molecular system, we find that relaxation from an initial configuration with the molecules arranged in a crystalline structure results in quite different temperatures for the internal (vibrational) and external (rotational and translational) modes. The coupling between internal and external modes in benzene is expected to be weak because of the large separation in frequency. Correspondingly the energy transfer between these modes also will be quite slow. Thus, translational and rotational modes will equilibrate more rapidly compared to the vibrational modes.

To achieve equilibration quickly, an isokinetic technique was applied to impose energy equipartition at a particular temperature-density state. The total kinetic energy of a system of N molecules can be separated as

$$K = K_x^{\text{cm}} + K_y^{\text{cm}} + K_z^{\text{cm}} + K^{\text{rot}} + K^{\text{vib}}. \tag{8}$$

The expectation values of the kinetic energy components for the benzene system (30 internal, 6 external degrees of freedom per molecule) are

$$\langle K_x^{\text{cm}}\rangle = \langle K_y^{\text{cm}}\rangle = \langle K_z^{\text{cm}}\rangle = \tfrac{1}{3}\langle K^{\text{rot}}\rangle = \tfrac{1}{30}\langle K^{\text{vib}}\rangle = \tfrac{1}{2}N_m k_B T, \tag{9}$$

where T is the desired temperature. In the isokinetic technique the five kinetic energy components are fixed at the expectation values by scaling the molecular velocities (atomic velocities in a molecular reference frame) and transforming back to atomic velocities (system reference frame). This scaling is carried out at each time step over a period of several thousand time steps until the time-averaged kinetic components appear stable and constant. In practice, this isokinetic technique is difficult to implement and computationally expensive to carry out for polyatomic molecules such as benzene. The main difficulty is in establishing the molecular reference frame for a flexible molecule. This reference frame is necessary for specifying the molecular–atomic velocity transformations separating the rotational and vibrational motions.

TABLE IV. Simulation cell dimensions for liquid and solid benzene.

State	Density (g/cm^3)	X (Å)	Y (Å)	Z (Å)
Solid, $T = 10$ K	1.114	14.58	18.94	13.48
Liquid, $T = 305$ K	0.874	16.81	16.81	16.81

In the present simulation a simplified equilibrium method was carried out where the center-of-mass kinetic energy components and a coupled rotational–vibrational component were maintained at their expected values for a specified temperature. This approach, while only approximate, worked reasonably well for achieving system equilibrium.

Two simulations have been carried out for a 32 molecule system, one in the liquid state at 305 K and density 0.874 g/cc, and the other in the solid state at 10 K and density 1.114 g/cc. The simulations were carried out in the microcanonical (N, V, E) ensemble with periodic boundary conditions. A fifth-order Nordsieck predictor-corrector algorithm was used to integrate the equations of motion, and the intermolecular interaction distance was limited to half the simulation cell side length. The integration time step was set at 3.1×10^{-4} ps.

For both the liquid and solid phase simulations, the initial configuration of the molecules was specified by using the known benzene crystalline structure (four molecules per unit cell),[20] but with the cell lengths adjusted to obtain the desired number density. The simulation cell dimensions for the solid and liquid runs are listed in Table IV. For the liquid phase simulation, the system was equilibrated over a period of 9 ps (29 500 time steps). The solid phase simulation was carried out at 10 K in order to analyze recent neutron scattering spectra for benzene at this temperature, but we have used cell dimensions and a density that correspond to a temperature of 78 K.[21] Below this temperature the benzene unit cell structure is not known and extrapolation of the cell dimensions to a 10 K state may be inaccurate. Following equilibration, both simulations were carried out for 15 ps (49 000 time steps). Results from the phase-space trajectory analysis are presented in the following section.

IV. MD RESULTS AND ANALYSIS

A. Structure

The structure of the benzene system was analyzed by calculating averages of molecular internal coordinates and intermolecular radial pair correlation functions. Although our interests are primarily in the investigation of the benzene vibrational properties, analysis of the structure is essential for verifying that the present potential model will maintain proper intra- and intermolecular structures.

Time-averaged molecular internal coordinates (equilibrium bond lengths and angles) for the liquid and solid phases are presented in Table V. The equilibrium values of the inter-

TABLE V. Time-averaged molecular internal coordinates for liquid (305 K) and solid (10 K) benzene[a]

Description[b]	Model[c]	$T = 10$ K	$T = 305$ K	Expt.[d]
CH stretch (r)	1.077	1.076	1.077	1.084
CC stretch (R)	1.395	1.394	1.395	1.397
CCH in-plane bend (β)	0.0	−0.01	0.0	0.0
CCC in-plane bend (α)	120.0	120.0	119.9	120.0
CH out-of-plane bend (γ)	0.0	0.0	0.0	0.0
CCCC dihedral bend (δ)	0.0	0.0	0.0	0.0

[a] Bond lengths in units of Å, bond angles in units of degrees.
[b] Molecular internal coordinates described in Fig. 1 and Table I.
[c] Reference 12.
[d] Reference 16.

nal coordinates used in the model, along with the experimentally accepted values for gaseous benzene,[16] are also included in this table for reference. It is observed that the model yields a structure that corresponds well with the experimentally determined conformational structure of the molecule and that the system is stable under normal thermal activation.

The intermolecular structure is shown in Figs. 2 and 3. In Fig. 2 the center-of-mass radial pair correlation functions $g_{gm}(r)$ for the solid and liquid phases are presented. For the solid phase, the first peak centered at 4.95 Å arises from the four symmetry-equivalent nearest neighbors. The second peak centered at 5.9 Å corresponds to the four second and third nearest neighbors. Correlations between equivalent molecules in different unit cells are partially observed at the truncation distance $L/2 = 6.75$ Å. For the liquid phase, the peaks observed in the solid phase are significantly broadened to produce a major single peak with its maximum at about 5.5 Å and its first minimum occurring at 7.5 Å (the truncation distance in the liquid case is $L/2 = 8.4$ Å). The coordination number of this peak is approximately 12. The minimum molecule–molecule separation distance is observed to be approximately 4.0 Å. In earlier simulations[3–6] of liquid benzene using LJ site–site potentials, the calculated $g_{cm}(r)$ exhibits a shoulder at 4.0 Å representing a stacked configuration where one molecule lies on top of the other. This configuration is considered to be less stable than configurations where the molecular symmetry axes are perpendicular and

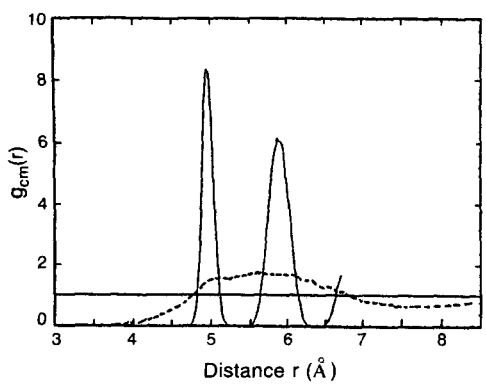

FIG. 2. Molecular center-of-mass radial pair correlation functions $g_{cm}(r)$ for liquid benzene at 305 K (- - -) and solid benzene at 10 K (—).

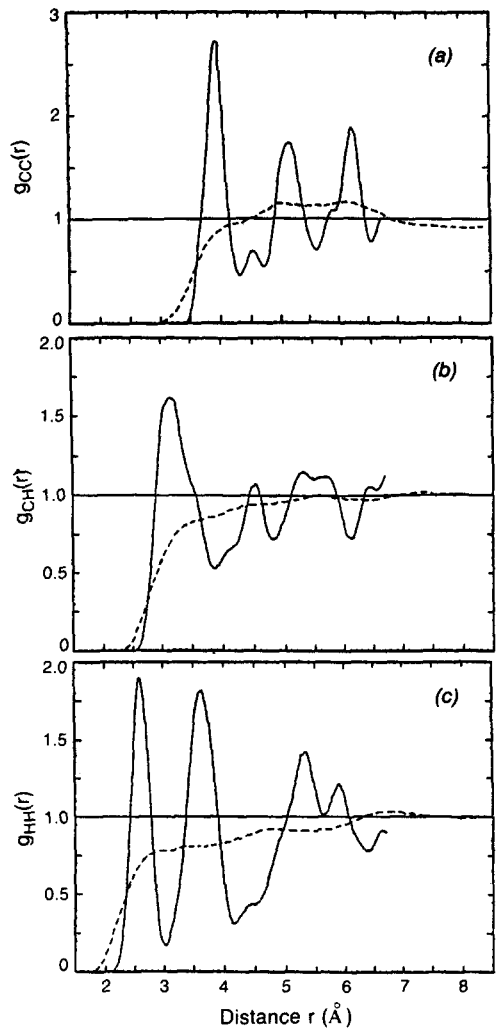

FIG. 3. Intermolecular radial pair correlation functions for liquid (- - -) and solid benzene (—): (a) $g_{CC}(r)$; (b) $g_{CH}(r)$; (c) $g_{HH}(r)$.

its occurrence should only be prominent at high densities.[9] Modification of the site–site potential function with the addition of a repulsive quadrupole–quadrupole interaction appears to reduce the occurrence of the stacked configuration, as evidenced by recent simulations.[5,7] A shoulder at 4.0 Å is not observed in the $g_{cm}(r)$ calculated in our work.

In Fig. 3 the atom–atom intermolecular radial pair correlation functions, $g_{CC}(r)$, $g_{CH}(r)$, and $g_{HH}(r)$ are shown. For the solid case, these correlation functions show a considerable amount of structure corresponding to the various nearest neighbors. For the liquid case there is significant broadening or smoothing out of these functions, although small oscillations still remain. This degree of broadening is to be expected, considering that for a given benzene dimer 36(72) atom–atom distances contribute to g_{CC}, g_{HH} (g_{CH}).

The intermolecular structure results presented here are consistent in terms of nearest neighbor distances and coordination numbers with previous simulation results.[3–7] It thus appears that the structural property $g(r)$ is not particularly sensitive to the difference between flexible and rigid molecule models. A similar observation has also been made for *n*-butane.[14]

B. Self-diffusion

A fundamental transport property of a liquid is diffusion. The self-diffusion coefficient D can be readily calculated from the MD simulation data using the Einstein relation,

$$D = \frac{1}{3} \lim_{\tau \to \infty} \frac{1}{2\tau} \langle |\mathbf{r}(\tau) - \mathbf{r}(0)|^2 \rangle, \tag{10}$$

where $\langle |r(\tau) - \mathbf{r}(0)|^2 \rangle$ is the mean-square displacement of a fixed point in a given molecule. Equivalently, the self-diffusion coefficient can also be obtained from the integral of the velocity autocorrelation function $\langle \mathbf{v}(t) \cdot \mathbf{v}(0) \rangle$,

$$D = \frac{1}{3} \lim_{\tau \to \infty} \int_0^\tau \langle \mathbf{v}(t) \cdot \mathbf{v}(0) \rangle dt. \tag{11}$$

In applying Eqs. (10) and (11) we take $\mathbf{r}(t)$ and $\mathbf{v}(t)$ to be the molecular center-of-mass positions and velocities, and the ensemble average $\langle \cdots \rangle$ is replaced in the usual manner by a suitable time average.

The center-of-mass mean-square displacement for liquid benzene at 305 K is shown in Fig. 4. After approximately 1.5 ps the displacement is seen to vary linearly with time, the signature of a diffusing particle. The corresponding self-diffusion coefficient is $D = 1.93 \pm 0.3 \times 10^{-5}$ cm^2/s. This value is slightly lower than the experimental values[22–24] at 305 K and 1 atm pressure which are in the range of 2.4–$2.7 \pm 0.1 \times 10^{-5}$. A value of $3.1 \pm 0.3 \times 10^{-5}$ at 312 K and 0.864 g/cc,[8] has been obtained in a rigid-molecule simulation, using a different potential function.

The center-of-mass mean-square displacement for solid benzene is also shown in Fig. 4. It is seen that this displacement is bounded and oscillatory; diffusion is clearly not taking placing on the time scale of the simulation.

In Fig. 5 the normalized center-of-mass velocity autocorrelation function for liquid benzene is shown. This quantity decays rapidly and becomes negative over a finite period of time. The negative correlation indicates a cage effect where the molecule is trapped by its nearest neighbors and partially reverses its direction of motion during this time. This is also indicated by the structure at finite frequencies in the Fourier transform of $c_{cm}(t)$ (see inset to Fig. 5). Beyond about 3 ps the autocorrelation function is probably dominated by noise. As a consistency check, we obtain a value of $1.83 \pm 0.3 \times 10^{-5}$ cm^2/s for D from Eq. (11).

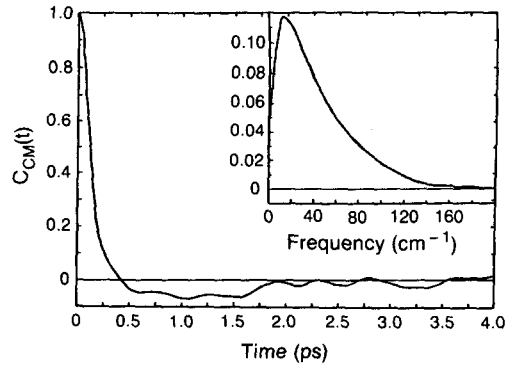

FIG. 5. Normalized velocity autocorrelation function of center-of-mass in liquid benzene. The frequency spectrum is shown in the inset.

C. Generalized frequency spectrum

The vibrational properties of a molecular system can be discussed in terms of the normalized velocity autocorrelation function $c(t)$ [cf. Eq. (11)],

$$c(t) = \langle \mathbf{v}(t) \cdot \mathbf{v}(0) \rangle / \langle \mathbf{v}(t) \cdot \mathbf{v}(0) \rangle, \tag{12}$$

where $\mathbf{v}(t)$ is the velocity of an atom or the molecular center-of-mass at time t. This quantity is essentially the second derivative of the mean-square displacement, and its Fourier transform $f(\omega)$ is the generalized frequency spectrum. Here generalization means that when $f(\omega)$ is interpreted as a vibrational density of states, it includes the square of the vibrational amplitudes.

Since we are dealing with an atomic model for the benzene molecule, we can construct $c(t)$ for the hydrogens (protons) and the carbons separately. The Fourier transforms of $c(t)$ will reveal the frequencies of vibrations, many of which have been observed by infrared and Raman spectroscopy. In the present analysis we consider only the hydrogens. By assuming that all hydrogens are dynamically equivalent, we can average $c(t)$ over all hydrogens in the system.

The resulting $c(t)$ in the liquid phase of benzene is displayed in Fig. 6. This function is seen to be highly oscillatory, reflecting a large range of characteristic frequencies. The solid phase result (not shown) is similar in appearance. The corresponding frequency spectra calculated from $c(t)$ without any data smoothing or filtering are shown in Figs. 7 and 8, respectively. The frequencies of external vibrations or molecular translations are expected to occur in the range 0–200 cm^{-1}, while the internal mode frequencies should extend

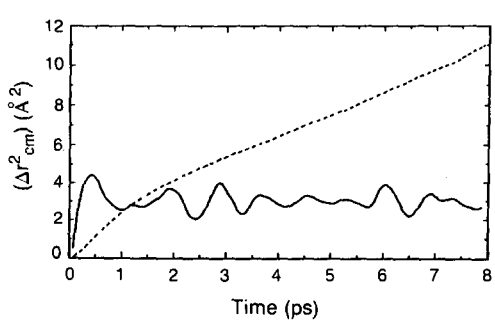

FIG. 4. Molecular center-of-mass mean-square displacements for liquid (- - -) and solid (—) benzene, the latter having been magnified by $\times 100$.

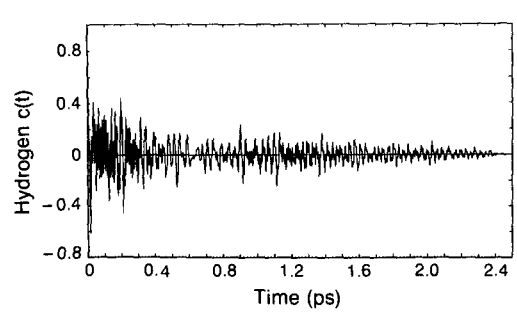

FIG. 6. Normalized velocity autocorrelation function of hydrogen atoms in liquid benzene.

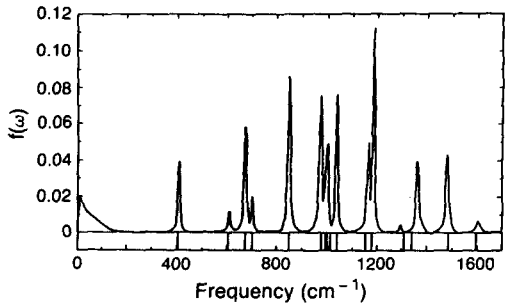

FIG. 7. Generalized frequency spectrum (in units of reciprocal frequency or cm) of hydrogen atoms in liquid benzene. Marks along the abscissa indicate experimental frequencies of normal mode vibrations (Ref. 27).

from about 400–3100 cm^{-1}. The lowest internal mode frequency at 404 cm^{-1} corresponds to the CCCC dihedral angle bending vibration, an assignment which we can make on the basis of a normal mode analysis (see below). Most of the internal mode vibrations occur in the frequency range 600–1600 cm^{-1}; these correspond to in-plane and out-of-plane bond stretching and bending. There are four high frequency modes occurring at $\sim$3070 cm^{-1} (not shown in Figs. 7 and 8) which correspond to CH stretching motions.

The internal mode frequencies obtained from the present simulations are tabulated in Table VI for the solid, liquid, and gas phases. In the case of the gas phase, a simulation of an isolated molecule was made and the vibrational frequencies obtained are compared to a normal mode analysis[25] using the same force field. The assignment of the MD frequencies is made using the atom displacements from the normal mode analysis. For reference, the experimentally observed gas[26] and liquid[27] phase frequencies are also listed in Table VI. There is an almost exact agreement between the normal mode frequencies and those obtained by simulation, the discrepancies in the high frequency modes being due to insufficient resolution of the simulation results ($\pm$ 3 cm^{-1}). This indicates that anharmonic effects are negligible. The overall agreement between the gas phase frequencies is excellent; largest deviations, occurring in the 1100–1300 cm^{-1} and 3000–3100 cm^{-1} regions, are less than 1%.

Comparison of the simulation data for the liquid and gas phases shows that no significant frequency shifts occur upon condensation. This is consistent with optical measurement results.[27] In comparing the liquid to the solid several slight frequency shifts, of the order $\pm$ 10 cm^{-1} and primarily at low frequencies, are seen in the simulation data. Infrared[28] and Raman[29,30] measurements on solid benzene show that there is good agreement between the liquid and solid phase frequencies, and only a few selected modes show significant frequency shifts upon a phase change. However, our comparison is made difficult by frequency splittings that occur in the solid. These splittings could be related to the shifts in the MD frequencies calculated in the solid phase.

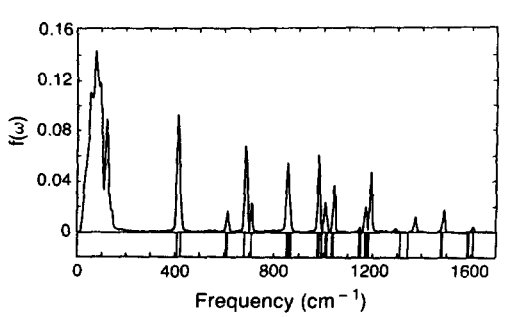

FIG. 8. Generalized frequency spectrum (in units of cm) of hydrogen atoms in solid benzene. Marks along the abscissa indicate experimental frequencies of normal mode vibrations (Refs. 28–30).

TABLE VI. Calculated and observed internal vibrational frequencies for benzene.[a]

Symmetry species		MD calc.[b] Solid 10 K	Liquid 305 K	Gas 500 K	Vib. analysis calc.	Liquid[c] expt. 298 K	Gas[d] expt.
In-plane modes							
e_{2g}	6	611	610	607	607	606	606
a_{1g}	1	(979)	(973)	(975)	983	992	993
b_{1u}	12	(1007)	(997)	(997)	997	1010	1010
e_{1u}	18	1043	1036	1036	1036	1037	1037
b_{2u}	15	1170	1165	1165	1162	1152	1146
e_{2g}	9	1192	1185	1185	1183	1178	1178
b_{2u}	14	1297	1297	1297	1297	~1310	1309
a_{2g}	3	1373	1363	1366	1366	~1340	1350
e_{1u}	19	1487	1482	1482	1482	1485	1482
e_{2g}	8	1607	1606	1607	1607	1596	1599
b_{1u}	13	(3062)	(3057)	(3057)	3051	3047	3057
e_{2g}	7	(3062)	(3057)	(3057)	3061	~3060	3056
e_{1u}	20	(3090)	3077	(3077)	3080	3062	3064
a_{1g}	2	(3090)	3102	(3077)	3095	3080	3073
Out-of-plane modes							
e_{2u}	16	413	408	402	402	405	404
a_{2u}	11	685	675	670	667	673	673
b_{2g}	4	708	705	700	701	703	707
e_{1g}	10	855	849	843	843	850	846
e_{2u}	17	(979)	(973)	(975)	969	975	967
b_{2g}	5	(1007)	(997)	(997)	996	995	990

[a] Frequencies in cm^{-1}; ( ) indicate particular mode unresolved—given frequency corresponds to centroid of major peak; ~ indicates there is some doubt concerning the precise value, usually because frequency has been inferred from combination bands or overtones.
[b] $d\omega \approx \pm 3$ cm^{-1}.
[c] Reference 27, $d\omega \approx \pm 2$ cm^{-1}.
[d] Reference 26, $d\omega \approx \pm 1$ cm^{-1}.

The simulation data for the external mode frequencies in the condensed phases are tabulated in Table VII, along with the experimental values. For the solid phase, four bands in the calculated spectrum (see Fig. 14) occurring at frequencies around 55, 76, 92, and 120 cm^{-1} agree reasonably well with experimentally observed frequencies. The shoulder at 32 cm^{-1} in the calculated spectrum should not be taken literally since the resolution in the $c(t)$ data is estimated to be about 20 cm^{-1}. Lattice frequencies observed in Raman[31–33] and far-infrared[34–36] measurements range from 53 to 136 cm^{-1} for low temperature benzene. Recent neutron scattering data[45,46] also show excitations in this range.

Extensive lattice dynamical calculations[37–39] at 140 K have been performed to analyze the optical measurements. These calculations produce four distinct bands at c a. 50, 78, 90, and 125 cm^{-1}. The interpretation based on the calculated eigenvectors is that these are due to acoustic (translatory), optical (translatory), C_6 and C_2 rotation, and C_2 rotation modes, respectively. Because the lattice mode

TABLE VII. Calculated and observed external vibrational frequencies for liquid and solid benzene.[a]

Solid benzene

Raman[b] $T=4$ K	$\nu_{obs.}$ i.i.n.s.[c] $T=9$ K	i.i.n.s.[d] $T=78$ K	$\nu_{calc.}$ MD $T=10$ K
	50	50	55
64	60		
69	72	75	76
86	90	85	92
100			
107			
136	125	120	120

Liquid benzene

Obs.[e]		MD calc.	
$\bar{\nu}$	$\nu_{h\omega}$[f]	$\bar{\nu}$	$\nu_{h\omega}$
78	91	40	70

[a] Frequencies in cm^{-1}.
[b] Reference 31.
[c] Reference 45.
[d] Reference 46.
[e] Reference 40.
[f] Full width at half-maximum.

frequencies are observed to be highly temperature dependent,[30] a detailed comparison of the simulation data at 10 K to the experimental results at 140 K should not be taken too seriously. On the other hand, with the exception of the low-frequency band at 32 cm^{-1}, the similarity between the calculated and observed lattice bands does signify a certain degree of reality of the simulation.

In contrast to the solid phase, the simulated frequency spectrum for liquid benzene shows a single broadband with a peak at about 20 cm^{-1} and a gradual decay to zero at approximately 150 cm^{-1}. The average frequency of the band is 40 cm^{-1}, and the width (FWHM) is 70 cm^{-1}. This result is not entirely consistent with optical[40] or neutron scattering[41] data. Low-frequency Raman measurements[40] on liquid benzene at 298 K show a single broadband centered at 78 cm^{-1} with a width of 91 cm^{-1}. Cold neutron measurements[41] of liquid benzene at 313 K have revealed a more detailed structure of the low frequency region. The data, when expressed in the form of $\omega^2 S_s(q,\omega)/q^2$ and extrapolated to $q=0$, show three distinct peaks occurring at 32, 71, and 104 cm^{-1}, with the middle peak being the most intense.

D. van Hove self-correlation function

Although optical data on vibrational frequencies are often used to test the validity of a force field, and to a certain extent the line intensity gives a measure of the vibrational amplitude, it remains true that very few intensity analyses are actually carried out. In the case of neutron scattering, intensity calculation is not a problem because the dynamic structure factor is a well defined quantity, one that can be evaluated once the atomic positions are known. For scattering samples that contain an appreciable amount of hydrogen, the analysis requires the van Hove self-correlation function since the scattering is predominantly incoherent and the measured scattering spectrum is proportional to the single-particle dynamic structure factor $S_s(q,\omega)$ of the protons. In turn S_s can be obtained as the double Fourier transform of the van Hove self-correlation function[42] $G_s(r,t)$,

$$S_S(q,\omega)=\frac{1}{2\pi}\int_{-\infty}^{\infty} dt\, e^{-i\omega t}F_s(q,t) \tag{13}$$

and

$$F_s(q,t)=\int d^3r\, e^{-i\mathbf{q}\cdot\mathbf{r}}G_s(r,t)$$

$$=\frac{1}{N}\sum_{l=1}^{N}\langle e^{i\mathbf{q}\cdot\mathbf{R}_l(t)}e^{-i\mathbf{q}\cdot\mathbf{R}_l(0)}\rangle, \tag{14}$$

where $\mathbf{R}_l(t)$ is the time-dependent position of the l th proton, $\hbar q$ and $\hbar\omega$ are the momentum and energy transfers to the neutron, and $\langle\ \rangle$ denotes a quantum mechanical average. Analysis of the van Hove self-correlation function therefore provides details of the single-particle dynamics of the protons including vibrational frequencies and amplitudes.

In order to calculate $S_s(q,\omega)$ from MD simulation, the intermediate scattering function $F_s(q,t)$ is directly evaluated in the classical limit using the calculated hydrogen atom trajectories. In the classical limit Eq. (14) goes to

$$F_s^{cl}(q,t)=\frac{1}{N}\sum_{l}^{N}\langle e^{-i\mathbf{q}\cdot[\mathbf{R}_l(t)-\mathbf{R}_l(0)]}\rangle \tag{15}$$

where $\langle\ \rangle$ now refers to a classical ensemble average. In this evaluation an angular average in q space is carried out by selecting

$$q=\frac{2\pi}{L}(n_x,n_y,n_z), \tag{16}$$

where L is the sidelength of the simulation cell and n_x, n_y, and n_z are a triplet of integers. These integers are selected such that the absolute value of Eq. (16) lies in a small interval dq centered about q. Typically, for large enough values of q, $F_s^{cl}(q,t)$ is averaged over 40 or more q vectors with $dq=0.1$ Å^{-1}. The hydrogens are again considered dynamically equivalent so that $F_s^{cl}(q,t)$ is also averaged over all the hydrogen atoms in the system. Following the evaluation of F_s^{cl}, the classical single-particle dynamic structure factor $S_s^{cl}(q,\omega)$ for the protons is evaluated by Eq. (13).

Because $F_s(q,t)$ and $S_s(q,\omega)$ are quantum mechanical quantities, certain known symmetry properties will not be preserved when $S_s(q,\omega)$ is evaluated using a classical ensemble average as in Eq. (15). The standard quasiclassical correction is[43]

$$S_s(q,\omega)=\exp(\hbar\omega/2k_BT)$$

$$\times\exp[-q^2\gamma(0)/2]S_s^{cl}(q,\omega). \tag{17}$$

The first exponential factor ensures the detailed balance condition is satisfied,

$$S_s(-q,-\omega)=\exp(-\hbar\omega/2k_BT)S_s(q,\omega). \tag{18}$$

The second exponential factor accounts for recoil effects with $\gamma(0)$, the mean-square displacement for the protons,

$$\gamma(0)=\frac{3k_BT}{m}\int_0^{\infty}d\omega\left[\cosh\left(\frac{\hbar\omega}{2k_BT}\right)-1\right]\frac{f(\omega)}{\omega^2}, \tag{19}$$

where $f(\omega)$ is the spectrum of the normalized velocity autocorrelation function of the protons. It should be noted that in

using Eq. (17) quantum corrections of order $\hbar^2$ and higher have been ignored.

To test the calculated $S_s(q,\omega)$ against the neutron spectra, the momentum and energy transfers of the experiment must be matched in the calculation. Experimental inelastic neutron scattering measurements on liquid[44] (299 K) and solid[45] (9 K) benzene have recently been carried out at the intense pulsed neutron source (IPNS), Argonne National Laboratory. The liquid measurements were made using the high resolution medium energy chopper spectrometer (HRMECS), operated in a constant-θ mode. In this mode the scattering angle θ is related to the momentum transfer $\hbar q$ according to

$$q = 0.695\left[2E_f + \hbar\omega - 2\sqrt{E_f(E_f+\hbar\omega)}\cos\theta\right]^{1/2}, \tag{20}$$

where q is in Å^{-1}, the scattered neutron energy $E_f = E_i - \hbar\omega$ is in meV, and the incident neutron energy is fixed at $E_i = 300$ meV. With the scattering angle held constant at $\theta = 6.94°$, and E_i fixed, q will vary with energy transfer $\hbar\omega$. We have generated a set of values for $F_s(q,t)$ and $S_s(q,\omega)$ at constant q for several q values spanning the experimental range (typically $1.5 < q < 5.2$ Å^{-1}) corresponding to $0 < \hbar\omega < 1700$ cm^{-1}. For each value of $\hbar\omega$, a corresponding value of q is obtained from Eq. (20), and $S_s(q,\omega)$ is then interpolated from the constant-q $S_s(q,\omega)$. The sequence of interpolated $S_s(q,\omega)$ at the experimental (q,ω) combination then becomes the function to be compared with experimental measurements.

$F_s^{\text{cl}}(q,t)$ for various values of q are presented in Fig. 9. It is observed that $F_s^{\text{cl}}(q,t)$ decreases with time in a smooth, continuous manner. As is generally true with wave number-dependent fluctuations, the decay rate is greater the shorter the wavelength of fluctuations. The corresponding frequency spectra are displayed in Fig. 10. $S_s^{\text{cl}}(q,\omega)$ is seen to have distinct structure at intermediate and high frequencies in correspondence with the short time ($t \leqslant 0.05$ ps) behavior of F_s^{cl}. Over the present range of q the structure is quite pronounced at small q and becomes smeared out into a broadband at high q.

Using the procedure just described, a theoretical spectrum of $S_s(q,\omega)$ for liquid benzene has been generated at

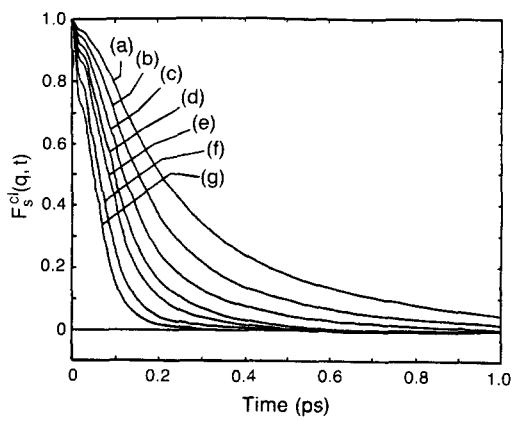

FIG. 9. Intermediate scattering function $F_s^{\text{cl}}(q,t)$ of hydrogen atoms in liquid benzene at q values of (a) 2.0; (b) 2.5; (c) 3.0; (d) 3.5; (e) 4.0; (f) 5.0; (g) 6.0 Å^{-1}.

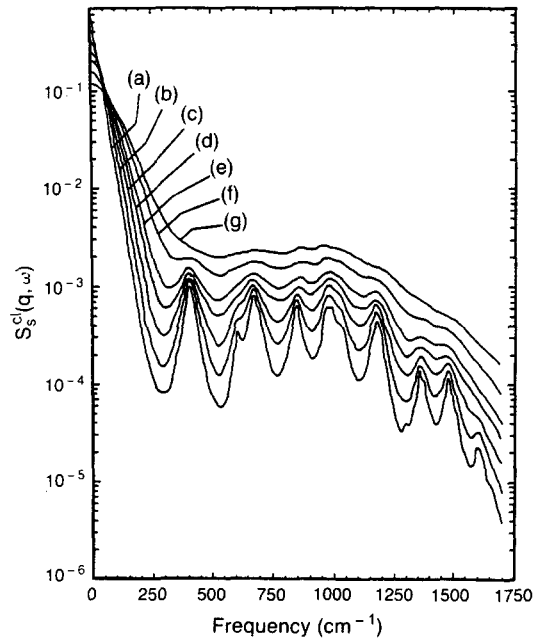

FIG 10. Dynamic structure factor $S_s^{\text{cl}}(q,\omega)$ (in units of cm) of hydrogen atoms in liquid benzene at the same q values as in Fig. 9.

values of (q,ω) that correspond to the HRMECS measurements. This spectrum is shown in Fig. 11 where the quantum corrections given by Eq. (17) have been applied. A value of $\gamma(0) = 0.31$ Å^{-2} was calculated from Eq. (19) using the velocity autocorrelation function shown in Fig. 6. The calculated $S_s(q,\omega)$ spectrum shows peaks that match well with the internal vibration modes. It should be noted that the elastic scattering intensity around $\omega = 0$ is orders of magnitude higher then the intensity of the remaining spectrum.

In Fig. 12 the calculated $S_s(q,\omega)$ is compared to the HRMECS spectrum for liquid benzene. The calculated spectrum has been resolution broadened with $\Delta E = 60$ cm^{-1}, which is approximately the experimental resolution at intermediate energy transfers. Because the experimental data are available only as relative intensities, the two spectra in Fig. 12 are normalized at the energy transfer $\hbar\omega = 1000$ cm^{-1}. Aside from this normalization, there are no adjustable parameters in the comparison.

The comparison shows there is qualitative agreement between the calculated and measured spectra in peak frequency and relative intensity. There are also clear differ-

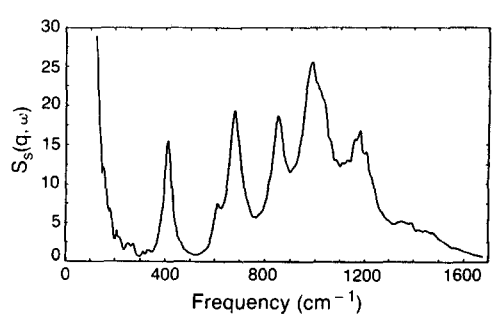

FIG. 11. Theoretical $S_s(q,\omega)$ (in units of cm) using (q,ω) values appropriate to HRMECS neutron inelastic scattering measurement on liquid benzene.

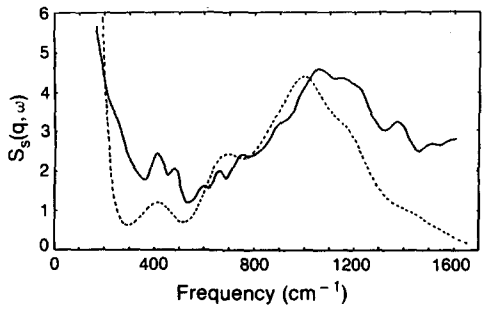

FIG. 12. Calculated (- - -) and experimental (—) $S_s(q,\omega)$ (in units of cm) for liquid benzene at 305 K. The calculated spectrum takes into account resolution broadening.

ences in the scattering intensity at energy transfer 400 cm^{-1} and for energy transfers beyond 1200 cm^{-1}. The discrepancy at 400 cm^{-1} could be due to an incomplete subtraction of the elastic scattering component in the experimental spectrum. For energy transfers beyond 1200 cm^{-1}, it is believed that the data contains a background contribution of unidentified origin.

For solid benzene the measurements were made using the crystal analyzer spectrometer (CAS) at the IPNS.[45] In this experiment, the spectrometer was operated in a constant-energy loss mode where the analyzer only detects scattered neutrons in a well-defined energy range. The q–ω relation can be taken to be approximately

$$q = 0.695\sqrt{7.48 + \hbar\omega}, \tag{21}$$

where q is in $Å^{-1}$ and the energy transfer $\hbar\omega$ is in meV. The measurements covered an energy range of $0 < \hbar\omega < 1000$ cm^{-1} with corresponding wave vector range of $1.5 < q < 8.0$ $Å^{-1}$. Data at 9 K are obtained in the form of double differential cross section. For comparison with simulation results we adopt the one-phonon scattering approximation[43]

$$\frac{d^2\sigma}{d\Omega\, d\omega} \propto \left(\frac{k_f}{k_i}\right)\frac{q^2}{\hbar\omega} f(\omega), \tag{22}$$

where $f(\omega)$ is the generalized frequency spectrum of the hydrogen atoms (see Fig. 8), and $\hbar k_f$, $\hbar k_i$ are the scattered and incident neutron momenta. At the present low temperature the one-phonon expression can be expected to be very accurate. Figure 13 shows the experimental data and the predicted cross section calculated according to Eq. (22). Normalization of the two curves is arbitrary. In Fig. 14 the region of lattice modes is shown in greater detail. Overall

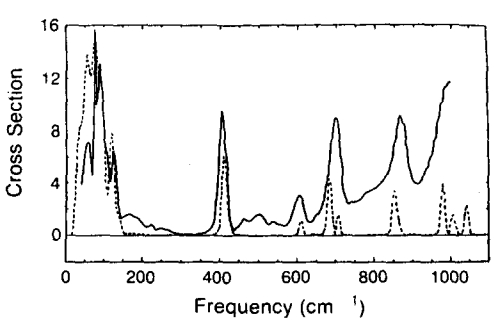

FIG. 13. Calculated (- - -) and experimental (—) scattering cross section for solid benzene at 10 K.

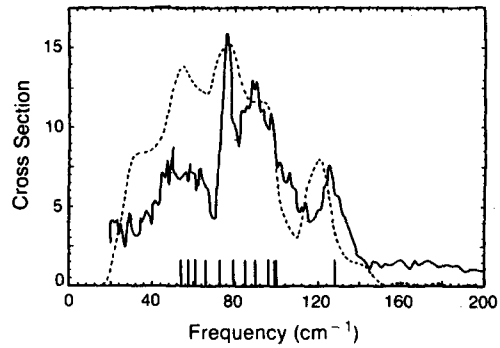

FIG. 14. Calculated (- - -) and experimental (—) scattering cross section in the lattice mode region for solid benzene. Marks along the abscissa indicate mode frequencies observed by optical spectroscopy.

agreement in the low-frequency region is quite good considering the rather rich structure of the spectrum. We are not certain that the overestimate of the scattering intensity in the region below ~70 cm^{-1} is significant; it would be interesting to investigate the sensitivity of this part of the spectrum first to the effect of system size and then to variations in the intermolecular potential parameters.

For energy transfers beyond 200 cm^{-1} Fig. 13 shows close correspondence between calculation and experiment. The measured spectrum appears to contain a component which becomes more intense at increasing energy transfer. We believe this is the major cause for the calculated peak intensities to be systematically lower than the observed values. It is true that multiphonon effects will contribute to a certain amount of background intensity. However, we do not think this is a plausible explanation because in the liquid spectrum (Fig. 12) there exists a similar discrepancy at large energy transfers and there multiphonon effects are included in the calculation. Thus the origin of the 'background' component in the experimental data remains to be clarified.

V. DISCUSSION

In this work we have carried out a molecular dynamics study of an atomistic model of benzene using a combination of *ab initio* force constants for bond stretching and bond angle bending, and atom–atom intermolecular potential functions. The dynamics of the fully flexible molecules in liquid and solid phases are analyzed in terms of the atomic motions of the hydrogens. Through the velocity autocorrelation function we obtain characteristic vibrational frequencies which match well with infrared and Raman data. By extending the analysis to wavelength-dependent density fluctuations we are able to calculate explicitly the dynamic structure factor, and hence the spectrum of inelastically scattered thermal neutrons. Since the simulation requires no assumptions other than classical Newtonian mechanics and a set of intra- and intermolecular forces, the present comparisons with experimental data enable us to make unambiguous inferences about the validity of the assumed potential model.

The question of adequacy of a potential model is difficult to resolve since there exist no general criteria, and in many instances the issue depends on the specific applications under consideration. In the context of vibrational properties

it is appropriate to require the potential model to give acceptable results for the frequencies and amplitudes of the internal as well as external modes to the extent that these have been measured by optical and neutron spectroscopy. On the basis of the direct confrontation between model predictions and experimental data presented in Figs. 7, 8, 12–14, we feel it is meaningful to conclude that the potential model we have adopted provides a description of the intra- and intermolecular forces that is sufficiently accurate for predictive applications. This is not to say that further refinements are not needed. For example, an understanding of the discrepancy in the frequency region 1300–1350 cm^{-1} in Figs. 7 and 8, would be quite desirable, as is a resolution of the intensity comparison around 400 cm^{-1} (Fig. 12) and 30–60 cm^{-1} (Fig. 14). In this respect, it would be of interest in future work to incorporate the effects of electrostatic interactions between partial charges[47] into the potential model.[48]

While our simulation system of 32 molecules may seem small at first glance, the number of interacting atoms, $N = 384$, is comparable to typical systems studied in atomic fluid simulations. For the vibrational properties, those at energies ~ 400 cm^{-1} and higher, we expect no significant N dependence in the results. On the other hand, it is conceivable that some size effects could be present in the low energy region, $\hbar\omega \lesssim 100$ cm^{-1}. As for the effects of long range interactions and correlations, a recent study of Stockmayer fluids showed that size effects in the dielectric constant are not observable for $N \gtrsim 108$.[49]

From the standpoint of simulating molecular systems, our atomistic model should be useful for testing the accuracy of rigid-molecule approximations. Also noteworthy are our calculations of the generalized frequency distribution and the dynamic structure factor for the range of frequencies covered and the level of resolution achieved. These results, taken together with those reported in Ref. 14, demonstrate the viability of simulating, as realistically as current knowledge of chemical forces and intermolecular interactions allows, the vibrational properties of alkanes and aromatic hydrocarbons. For an in-depth study of the structural phases of an alkane, see Ref. 48.

ACKNOWLEDGMENTS

One of us (J.A.) gratefully acknowledges a Schlumberger–Doll Fellowship as well as summer employment at Schlumberger–Doll Research. We would like to thank G. S. Pawley for sending us preprints of the work cited in Ref. 48. We wish to thank W. Nelligan, D. LePoire, S. H. Chen, T. Brun, C. Loong, D. Price, and R. Kelb for the use of their experimental data prior to publication.

APPENDIX A: CALCULATION OF *B* MATRIX ELEMENTS

The B matrix is used to transform molecular internal coordinates to Cartesian coordinates. The elements of B are derived by the Wilson S vector technique.[15] For the benzene internal coordinate description there are four types of internal coordinates considered: bond stretch, valence angle bend, out-of-plane wag, and torsional bend. Unit vectors along the bond lengths, $\mathbf{e}_{ij}$, are expressed in Cartesian coordinates as

$$\mathbf{e}_{ij} = [(x_j - x_i)\mathbf{i} + (y_j - y_i)\mathbf{j} + (z_j - z_i)\mathbf{k}]\frac{1}{r_{ij}}$$

where r_{ij} is the distance between atoms i and j.

1. Bond stretch

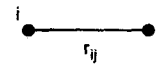

$$r_{ij} = [(x_j - x_i)^2 + (y_j - y_i)^2 + (z_j - z_i)^2]^{1/2}.$$

S vectors for atoms i and j:

$$\mathbf{S}_i = -\mathbf{e}_{ij},$$

$$\mathbf{S}_j = \mathbf{e}_{ij}.$$

2. Valence angle bend

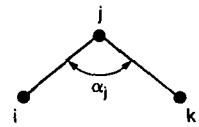

$$\alpha_j = \cos^{-1}[-\mathbf{e}_{ij}\cdot\mathbf{e}_{jk}], \quad \alpha_j \neq \pi.$$

S vectors for atoms i, k, and j:

$$\mathbf{S}_i = \frac{\cos(\alpha_j)\mathbf{e}_{ji} - \mathbf{e}_{jk}}{r_{ij}\sin(\alpha_j)},$$

$$\mathbf{S}_i = \frac{\cos(\alpha_j)\mathbf{e}_{jk} - \mathbf{e}_{ji}}{r_{jk}\sin(\alpha_j)},$$

$$\mathbf{S}_j = -(\mathbf{S}_i + \mathbf{S}_k).$$

3. Out-of-plane wag

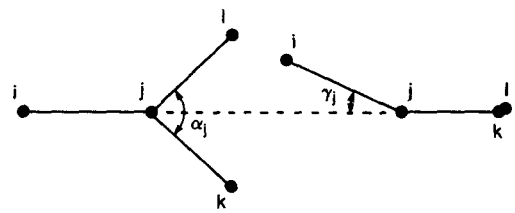

$$\gamma_i = \sin^{-1}\left[\mathbf{e}_{ji}\cdot(\mathbf{e}_{jk}\times\mathbf{e}_{jl})\frac{1}{\sin(\alpha_j)}\right], \quad \gamma_i \neq \pi/2.$$

S vectors for atoms i, k, l, and j:

$$\mathbf{S}_i = \frac{1}{r_{ji}}\left[\frac{\mathbf{e}_{jk}\times\mathbf{e}_{jl}}{\sin(\alpha_j)\cos(\gamma_i)} - \tan(\gamma_i)\mathbf{e}_{ji}\right],$$

$$\mathbf{S}_k = \frac{1}{r_{jk}}\left\{\frac{\mathbf{e}_{jl}\times\mathbf{e}_{ji}}{\sin(\alpha_j)\cos(\gamma_i)} - \frac{\tan(\gamma_i)}{\sin^2(\alpha_j)}[\mathbf{e}_{jk} - \cos(\alpha_j)\mathbf{e}_{jl}]\right\},$$

$$\mathbf{S}_l = \frac{1}{r_{jl}}\left\{\frac{\mathbf{e}_{ji}\times\mathbf{e}_{jk}}{\sin(\alpha_j)\cos(\gamma_i)} - \frac{\tan(\gamma_i)}{\sin^2(\alpha_j)}[\mathbf{e}_{jl} - \cos(\alpha_j)\mathbf{e}_{jk}]\right\},$$

$$\mathbf{S}_j = -(\mathbf{S}_i + \mathbf{S}_k + \mathbf{S}_l).$$

4. Torsional bend

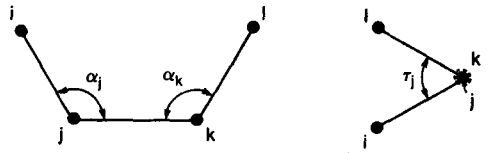

$$\tau_j = \mathrm{sgn}\left(\mathbf{e}_{ij}\cdot\frac{\mathbf{e}_{jk}\times\mathbf{e}_{kl}}{\sin(\alpha_k)}\right)\cos^{-1}\left[\frac{(\mathbf{e}_{ij}\times\mathbf{e}_{jk})\cdot(\mathbf{e}_{jk}\times\mathbf{e}_{kl})}{\sin(\alpha_j)\sin(\alpha_k)}\right],$$

$$-\pi < \tau_j \leqslant \pi$$

S vectors for atoms i, j, k, and l:

$$\mathbf{S}_i = -\frac{\mathbf{e}_{ij}\times\mathbf{e}_{jk}}{r_{ij}\sin^2(\alpha_j)},$$

$$\mathbf{S}_j = \frac{(r_{jk} - r_{ij}\cos(\alpha_j))(\mathbf{e}_{ij}\times\mathbf{e}_{jk})}{r_{jk}r_{ij}\sin^2(\alpha_j)} - \frac{\cos(\alpha_k)(\mathbf{e}_{jk}\times\mathbf{e}_{kl})}{r_{jk}\sin^2(\alpha_k)},$$

$$\mathbf{S}_k = -\frac{[r_{jk} - r_{kl}\cos(\alpha_k)](e_{jk}\times\mathbf{e}_{kl})}{r_{jk}r_{kl}\sin^2(\alpha_k)} + \frac{\cos(\alpha_j)(\mathbf{e}_{ij}\times\mathbf{e}_{jk})}{r_{jk}\sin^2(\alpha_j)},$$

$$\mathbf{S}_l = \frac{\mathbf{e}_{jk}\times\mathbf{e}_{kl}}{r_{kl}\sin^2(\alpha_k)}.$$

The S vectors are evaluated given the Cartesian coordinates of the atoms in the molecule. The components of the S vectors correspond to the B matrix elements. The location of the S components in B depends on the definition of **R**, the internal coordinate vector.

[1]For a review, see D. Levesque, J. J. Weis, and J.-P. Hansen, Topics Cur. Phys. **36**, 37 (1984).
[2]D. J. Tildesley, in *Molecular Liquids—Dynamics and Interactions*, edited by A. J. Barnes, W. J. Orville-Thomas, and J. Yarwood (Riedel, Dordrecht, 1984), p. 519.
[3]D. J. Evans and R. O. Watts, Mol. Phys. **32**, 93 (1976).
[4]O. Steinhauser, Chem. Phys. **73**, 155 (1982).
[5]M. Claessens, M. Ferrario, and J.-P. Ryckaert, Mol. Phys. **50**, 217 (1983).
[6]F. Serrano Adan, A. Banon, and J. Santamaria, Chem. Phys. **86**, 433 (1984).
[7]P. Linse, J. Am. Chem. Soc. **106**, 5425 (1984).
[8]P. Linse, S. Engstrom, and B. Jonsso, Chem. Phys. Lett. **115**, 95 (1985).
[9]D. J. Evans and R. O. Watts, Mol. Phys. **29**, 777 (1975); **31**, 83 (1976).
[10]A. H. Narten, J. Chem. Phys. **67**, 2102 (1977).
[11]G. Karlstrom, P. Linse, A. Wallquist, and B. Jonsson, J. Am. Chem. Soc. **105**, 3777 (1983).
[12]P. Pulay, G. Fogarasi, and J. E. Boggs, J. Chem. Phys. **74**, 3999 (1981).
[13]B. M. Powell, G. Dolling, and H. Bonadeo, J. Chem. Phys. **69**, 2428 (1978).
[14]J. J. Ullo and S. Yip, J. Chem. Phys. **85**, 4056 (1986). For another recent MD study of *n*-butane, see Ref. 48.
[15]E. B. Wilson, Jr., J. C. Decius, and P. C. Cross, *Molecular Vibrations* (McGraw-Hill, New York, 1955).
[16]A. Langseth and P. B. Stoicheff, Can. J. Phys. **34**, 350 (1956).
[17]D. E. Williams, J. Chem. Phys. **45**, 3770 (1966).
[18]D. E. Williams, J. Chem. Phys. **47**, 4680 (1967).
[19]For a recent review, see D. Fincham and D. M. Hayes, Adv. Chem. Phys. **63**, 493 (1985).
[20]G. E. Bacon, N. A. Curry, and S. A. Wilson, Proc. R. Soc. London Ser. A **279**, 98 (1964).
[21]B. M. Kojen, Zhur. Fiz. Khim. **28**, 566 (1954).
[22]D. R. Falcone, D. C. Douglass, and D. W. McCall, J. Phys. Chem. **71**, 2754 (1967).
[23]M. A. McCool, A. F. Collings, and L. A. Woolf, J. Chem. Soc. Faraday Trans. 1 **68**, 1489 (1972).
[24]P. Stilbs and M. E. Moseley, Chem. Scripta **15**, 176 (1980).
[25]The benzene normal mode vibration analysis was carried out using the Wilson GF method, described in Ref. 15. This analysis used the computer programs developed by D. F. McIntosh and M. R. Peterson, QCPE Program 32, Quantum Chemistry Program Exchange, Indiana University (1977).
[26]S. Brodersen and A. Langseth, K. Dan. Vidensk. Selsk. Mat.-Fys. Sk. **1**, No. 1 (1956).
[27]F. A. Miller, J. Chem. Phys. **24**, 996 (1956).
[28]J. L. Hollenberg and D. A. Dows, J. Chem. Phys. **37**, 1300 (1962).
[29]M. Ito, J. Chem. Phys. **42**, 2844 (1965).
[30]A. R. Gee and G. W. Robinson, J. Chem. Phys. **46**, 4847 (1967).
[31]M. Ito and T. Shigeoka, Spectrochim. Acta **22**, 1029 (1966).
[32]H. Bonadeo, M. P. Marzocchi, E. Castellucci, and S. Califano, J. Chem. Phys. **57**, 4299 (1972).
[33]W. Ellenson and M. Nicol, J. Chem. Phys. **61**, 1380 (1974).
[34]I. Harada and T. Shimanouchi, J. Chem. Phys. **46**, 2708 (1967).
[35]G. W. Chantry, H. A. Gebbie, B. Lassier, and G. Wyllie, Nature (London) **214**, 163 (1967).
[36]B. Wyncke and A. Hadni, C. R. Acad. Sci. B **275**, 825 (1972).
[37]M. Nakamura and T. Miyazawa, J. Chem. Phys. **51**, 3146 (1969).
[38]G. Taddei, H. Bonadeo, M. P. Marzocchi, and S. Califano, J. Chem. Phys. **58**, 966 (1973).
[39]H. Bonadeo and G. Taddei, J. Chem. Phys. **58**, 979 (1973).
[40]M. Perrot, M. H. Brooker, and J. Lascombe, J. Chem. Phys. **74**, 2787 (1981).
[41]V. Trepadus, S. Rapeanu, I. Padoreanu, V. A. Parfenov, and A. G. Novikov, J. Chem. Phys. **60**, 2832 (1974).
[42]L. van Hove, Phys. Rev. **95**, 249 (1954).
[43]H. Boutin and S. Yip, *Molecular Spectroscopy with Neutrons* (MIT, Cambridge, MA 1968).
[44]W. Nelligan, D. LePoire, S.-H. Chen, C. Loong, and D.-L. Price (unpublished data, 1984).
[45]T. Brun, W. Nelligan, D. LePoire, and R. Kleb (unpublished data, 1984).
[46]E. L. Bokhenkov, V. G. Fedotov, E. F. Sheka, I. Natkaniec, M. Sudnik-Hrynkiewicz, S. Califano, and R. Righini, Nuovo Cimento B **44**, 324 (1978).
[47]T. L. Starr and D. E. Williams, Acta Crystallogr. Sect. A **33**, 771 (1977).
[48]An extensive molecular dynamics study of orientational disorder and plastic phase transition in *n*-butane has been recently performed using a system of 2048 molecules in which the methyl and methylene groups are treated as rigid and torsions about the C–C bonds are allowed, K. Refson, Ph.D. thesis, University of Edinburgh, 1985; K. Refson and G. S. Pawley (to be published). Nonbonded atom–atom potential of the same form as adopted here is used along with a potential for dihedral bond rotation. Some calculations also include the Coulomb interactions the effects of which are found to be small.
[49]C. G. Gray, Y. S. Sainger, C. G. Joslin, P. T. Cummings, and S. Goldman, J. Chem. Phys. **85**, 1502 (1986).